2011

Transducer characterization for Vibrothermography

Jyani Somayajulu Vaddi
Iowa State University

Transducer characterization for Vibrothermography

by

Jyani Somayajulu Vaddi

A thesis submitted to the graduate faculty

in partial fulfillment of the requirements for the degree of

MASTER OF SCIENCE

Major: Engineering Mechanics

Program of Study Committee:

Stephen D. Holland, Major Professor

Lester W. Schmerr

Thomas J. Rudolphi

Iowa State University

Ames, Iowa

2011

TABLE OF CONTENTS

LIST OF TABLES

LIST OF FIGURES

ACKNOWLEDGEMENTS

This material is based upon work supported by Thermal Wave Imaging, Inc. under an STTR contract by the US Navy (Federal Agency) and performed at the Center for Nondestructive Evaluation at Iowa State University.

I am indebted to my major professor Dr. Stephen D. Holland for providing me with an opportunity to learn and do research and for guiding me with extreme patience and encouragement.

I am grateful to the members of my programme of study committee Dr. Lester W. Schmerr and Dr. Thomas J. Rudolphi for their review and invaluable suggestions on the thesis.

I sincerely thank my colleague Ricky Reusser for helping me all through this project with his contributions. I would like to thank my peers at CNDE, Jon Anderegg, Wenjun Zhang, Jeremy Renshaw and many others for their support. I would like to thank my friend Pooja Paranjape for her invaluable comments on the thesis.

I would like to extend my gratitude to my mother and my brother, who stood by me and supported me at every moment. I am thankful for the support of all my friends, without which none of this would have been possible.

ABSTRACT

Vibrothermography, also known as Sonic IR and Thermosonics, is an NDE technique for finding cracks and flaws based on vibration-induced frictional rubbing of unbonded surfaces. The vibration is usually generated by a piezoelectric stack transducer which transduces electrical energy into large amplitude mechanical vibrations. The purpose of this study is to develop an understanding of the excitation process for vibrothermography so that optimal parameters and transducers for the testing can be selected. The amplitude and impedance transfer characteristics of the transducer system control the vibration of the sample. Within a linear contact (no tip chatter) model, the interaction between the transducer system and the specimen can be characterized using the theory of linear time-invariant (LTI) systems and electro-mechanical Norton equivalence.

This work presents quantitative measurements of the performance of piezoelectric stack transducers in a vibrothermography excitation system and the effect of transducer performance and specimen characteristics on the induced vibration in the specimen. We show that with compliant coupling, the specimen vibration is directly proportional to the transducer open circuit velocity and that the system resonances generated because of metal-metal contact of specimen and transducer are disconnected by adding a couplant between specimen and transducer. We then give suggestions for transducer and couplant selection for vibrothermography and suggest methods to flatten the velocity spectrum of the transducer.

We extend our analysis to high amplitude transducer behavior and elaborate on the effect of power amplifier saturation on the transducer behavior. The saturation effect negates the effect of adding an external inductance to flatten the transducer velocity spectrum. Finally, preliminary results are reported on the effect of transducer degradation phenomenon.

CHAPTER 1. INTRODUCTION

Vibrothermography is a nondestructive evaluation(NDE) technique for finding cracks and delaminations in materials by vibration induced crack heating. When a specimen is vibrated at high amplitudes and if it has a defect (eg: cracks, delaminations), the two contacting surfaces of the defect rub against each other and heat is generated locally because of the friction between these two rubbing surfaces. This method is also called Sonic IR, Thermosonics and Vibroacoustics. Vibrothermography was first developed by Henekke *et al.* during early 1980s [1]. Several research groups have been investigating this method ever since. This technique has shown substantial promise as an alternative to Fluorescent Penetrant Inspection (FPI) for turbine components. Unlike FPI, vibrothermography does not involve chemicals and it can detect cracks even under a thermal barrier coating. However, the underlying physics of this method is not completely understood and the current practices do not yet yield the desired level of repeatability.

Defect detection in vibrothermography depends on several factors like crack size[2], dynamic stress[2], excitation frequency[3, 4], loading mode[5], crack closure [6] etc. A key prerequisite for studying some of these factors is consistent and repeatable vibration generation. High enough amplitude vibrations should be coupled into the specimen so that adequate dynamic stress levels for crack detection are reached. On the other hand, excessively high amplitude vibrations might run the risk of damaging the specimen [7]. In this thesis, we analyze the excitation system we use here at Iowa State University (ISU)'s Center for Nondestructive Evaluation (CNDE) and give recommendations on optimizing the transducer parameters to achieve successful defect detection and maximum transducer efficiency.

The most common excitation source used for vibrothermography is an ultrasonic welder. These devices are widely used in plastics and packaging industry. An ultrasonic welder consists

of a piezoelectric transducer(converter) with a booster that acts as a mounting point, an acoustic horn to amplify and efficiently couple the energy into the specimen, and a power source that drives the system. The transducer assembly is finely tuned to resonate at a single narrowband frequency. The operating parameters for ultrasonic welders are operating frequency and power levels desired. The specimen to be inspected is attached to the tip of the horn with a soft coupling material between the tip and the contact surface and vibrated at high amplitude to cause vibrothermographic heating[8]. Because the contact of the transducer tip and specimen is often nonlinear, different harmonics and sub-harmonics can be generated which often excite one or more natural resonances of the specimen. It is the high amplitude vibrations at these resonances that tend to make any defects heat up. The generation of unusual subharmonics often needed to match resonance is characteristic of non linear acoustic chaos[9]. The generation of acoustic chaos is inherently non-repeatable and may result in poor reproducibility of overall testing. However, the generation of acoustic chaos is reported to be vital in defect detection with this type of excitation and enhances the defect heating[9]. The downside, however with this type of excitation is that because it is non-repeatable, it is not very useful for developing conclusions pertaining to the underlying physics.

As an alternative, we use a broadband excitation system at ISU's CNDE that, instead of exciting the specimen at a single welder operating frequency and relying on acoustic chaos generation, can operate at a wide bandwidth, thus making it possible to explicitly excite the specimen at specimen's natural frequency[10]. This excitation system consists of a high power broadband piezo stack transducer operated along with a power amplifier. Because of their relatively wide bandwidth, these transducers can be tuned electronically to excite the specimen explicity at its resonance frequencies and therefore it is possible to achieve high vibration amplitude and hence better crack heating at the specimen resonances [1]. For certain geometries, the specimen vibration can be analyzed using elementary flexural wave theory[11] and therefore quantitative results comparing dynamic stress to crack heating can be obtained. The selection parameters for these transducers are stack length, stack diameter, preload and manufacturer. Stack length determines natural resonances of the transducer. Stack diameter determines the stiffness of transducer. Longer transducers have smaller resonance frequencies and higher stroke

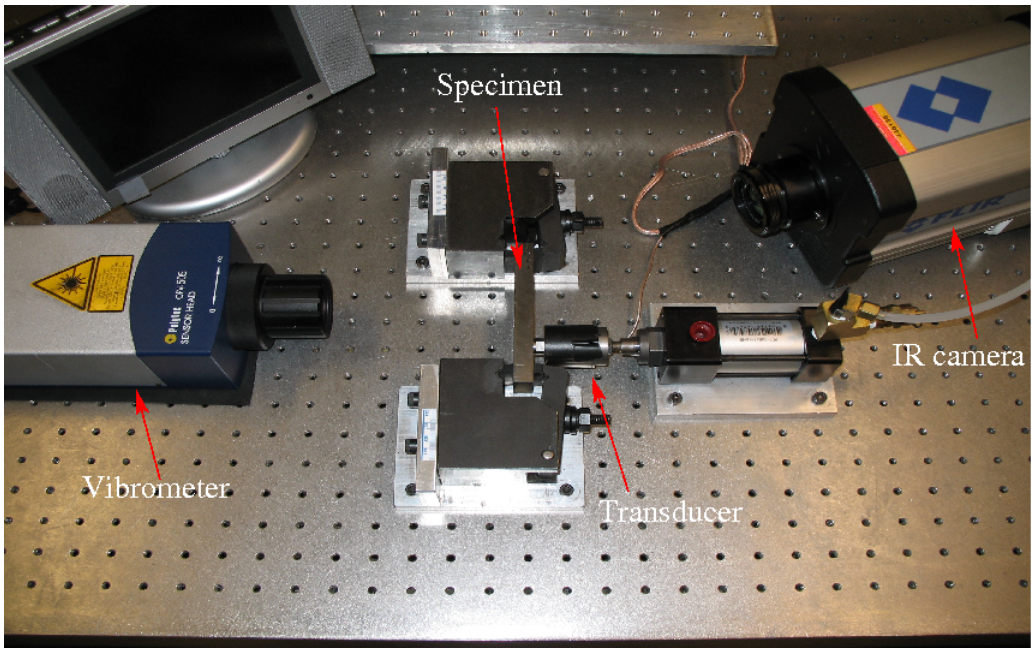

Figure 1.1 A picture of the vibrothermography set up used at Iowa State University's Center for Nondestructive evaluation.

lengths than shorter ones. Thicker transducers have more stiffness and can be used with heavier loads. Fig. 1.1 shows a picture of the vibrothermography system we use at ISU's CNDE.

In this thesis, in the remainder of the introduction, we explain the excitation system we use for vibrothermography. In chapter 2, we explain the characterization of the broadband piezoelectric stack transducers in the context of vibrothermography and suggest parameters for transducer selection to optimize the overall efficiency of vibration generation and the transducer system. We first discuss the small signal linear analysis of the transducer and derive results on transducer-specimen interaction and the role played by the couplant. We then suggest criteria for selection in terms of the transducer parameters (stack length and stack diameter) and how to improve the usable bandwidth of these transducers.

In chapter 3, we extend our analysis to the high amplitude vibrations and the phenomenon of power amplifier saturation. Some power amplifiers (like McIntosh MC1201) saturate before the short term damage threshold of the transducer is reached. This constrains the operational limits of the transducer. On the other hand, very high amplitude operation of transducers results in long term degradation of the piezo stack. With prolonged use at high amplitude

excitations, the transducer spectrum changes as the transducer degrades. We shall discuss briefly, this phenomenon before concluding the study.

1.1 Hardware Description

The hardware for a vibrothermography experiment consists of an excitation system for generating mechanical vibrations in the specimen and a measurement system to measure the specimen vibrations and the heat generated. We use high power piezoelectric broadband transducers for mechanical vibration generation at ISU's Center for nondestructive evaluation. The principle behind the functioning of these piezoelectric stack transducers is the 'Piezoelectric effect', a property whereby materials deform mechanically in response to an electric field and in turn produce an electric potential when deformed mechanically. A piezo stack transducer has a stack of disk-like piezoelectric elements housed in a stainless steel casing, often with a compressive preload. When a voltage is applied across the ends of the transducer, the stack deforms axially generating a stroke like motion. So, one can think of these transducers as 'moving capacitors'. In this study, we used 10 transducers of different geometries from two manufacturers, Piezomechanik gmbh and Physik Instrumente Inc, 5 from each. We name these 'MMddll', where MM is the manufacturer (PM for piezomechanik, PI for Physik Instrumente), dd is the stack diameter (16,25,35) in mm and ll is the stack length (20,40,60) in mm and use this naming for the rest of this thesis. The details of these transducers are given in table 1.1. Fig. 1.2 shows pictures of two of the transducers (PI2533 and PM2540) we used for this study.

The high power Piezomechanik transducers used for this study are specified for voltage range of -200 to 1000V while the Physik Instrumente transducers are specified for a voltage range of 0 to 1000V. We use a Tabor ww5061 waveform generator to generate the customized AC waveforms for exciting the transducer. The excitation signal is fed to the arbitrary waveform generator via a network interface. A McIntosh MC1201 (maximum rated power of 1.2KW) audio power amplifier amplifies the generated waveform and a custom built +/- 500V DC bias generator adds a 500V bias to this amplified waveform. The DC bias is for the transducer to keep the voltage with in the 0 to 1000V or -200 to 1000V manufacturer specifications of the transducer. The voltage and current across the transducer are measured with custom built

Table 1.1 Table showing the details of transducers used for this study.

Manufacturer	**Name**	**stack dia(mm)**	**stack length(mm)**	**Mfg Part No.**
Piezomechanik Gmbh	PM1620	16	20	PSt 1000/16/20 VS25
	PM1660	16	60	PSt 1000/16/60 VS25
	PM2540	25	40	PSt 1000/25/40 VS35
	PM3520	35	20	PSt 1000/35/20 VS45
	PM3560	35	60	PSt 1000/35/60 VS45
Physik Instrumente Inc	PI1631	16	31	P-216.20
	PI2520	25	20	P-225.10
	PI2533	25	33	P-225.20
	PI2560	25	60	P-225.40
	PI3534	35	34	P-235.20

Figure 1.2 Picture showing close up of two of the transducers used for this study. On the left is a Physik Instrumente transducer (PI2533) with stack length 33 mm and stack diameter 25 mm and on the right is a Piezomechanik transducer (PM2540) with stack length 40 mm and stack diameter 25 mm.

voltage and current sensors. Fig. 1.3 shows the schematic diagram of the vibrothermography excitation system we use at the ISU's Center for NDE. A Polytec Laser doppler vibrometer measures the velocity of generated vibrations. A microphone can be used in place of the vibrometer for lower cost vibration measurement. A Flir SC6000 infrared camera captures the infrared images during the test. These images are post processed to detect any defects in the specimen. A trigger generator module was developed at ISU's CNDE that generates trigger signals for waveform generator, infrared camera and the data acquisition card. A DAS4020 data acquisition card is used for aquiring the various waveforms. An EDT PCI image acquisition card captures the frames from the infrared camera.

We use a software package called 'Dataguzzler', a custom built laboratory data acquisition software as the computer interface for performing various experiments. Dataguzzler has modules that control different hardware equipments via command line interface. Dataguzzler has capabilities to capture, store and process the data in real time. Apart from the basic features like background subtraction, Fourier analysis and basic math operations, it also has some advanced image processing capabilities.

All the calculations and data analysis were performed in the Python programming language.

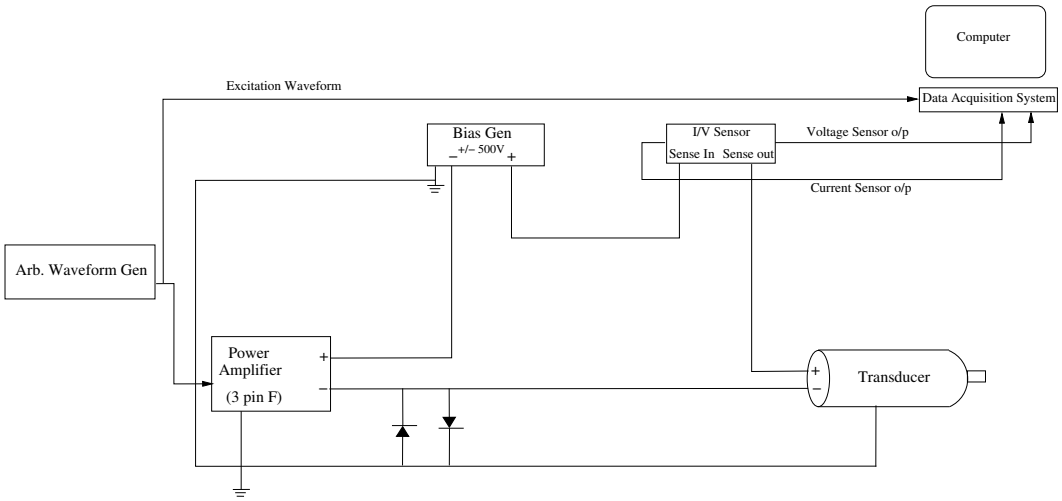

Figure 1.3 Schematic of the excitation system used for Vibrothermography. The arbitrary waveform generator generates the desired waveform, which the power amplifier amplifies. A +/- 500V DC bias generator adds a bias voltage to the amplified waveform to meet the transducer manufacturing specifications. The current and voltage sensors measure the respective quantities and are displayed on dataguzzler interface via data acquisition card.

CHAPTER 2. SMALL SIGNAL TRANSDUCER ANALYSIS

The principal component of any excitation system for vibrothermography is a transducer to generate mechanical vibrations. Usually, high power piezoelectric transducers are used for vibration generation. As the name suggests, these transducers are made of piezoelectric materials. The underlying principle of this type of transducer is 'Piezoelectric effect', which is an interaction between electrical and mechanical systems. The direct piezoelectric effect is when electric polarization is produced by mechanical stress. Closely related to it is its converse effect, whereby a crystal becomes strained when an electric field is applied. Both effects are manifestations of the same fundamental property of the crystal[12]. Some commonly used piezoelectric materials in transducers are Lead zirconate titanate (PZT), Barium titanate, etc. The broadband piezoelectric stack transducers we used for this study are made of PZT disks stacked together with a compressive preload.

It is important to analyze the transducer characteristics to understand the role played by excitation sources in vibrothermography, In this chapter, we model the broadband piezoelectric stack transducer as a linear system and characterize its behavior based on three parameters, open circuit velocity, mobility and immovable object force. Using these parameters, we explain the behavior of specimen, the interaction between transducer-specimen system and the role played by the so called 'couplant' used in vibrothermography. We then give criteria for transducer selection and recommendations for improving the transducer response.

2.1 Transducer as a LTI two port model

Although inherently non linear at high excitation amplitudes, piezoelectric materials behave linearly and can be modeled as a linear system at sufficiently low amplitudes. We model the

piezo stack transducer as an electromechanical LTI (Linear Time Invariant) two port network, the input port of which is electrical and output port, mechanical[12]. The control variables are current and voltage on the electrical end and force and velocity on mechanical end. This type of model can be characterized by four network parameters; two of which correspond to impedances and the other two correspond to electromechanical coupling coefficients. To map the mechanical quantities with their electrical analogs, we follow a mobility analogy, in which force maps to current and velocity maps to voltage[13]. The reason for using mobility analogy for our analysis is that the mechanical force balance, $\sum_i F_i = 0$ at a node is analogous to Kirchoff's Current Law (KCL) in electrical circuits, $\sum_i I_i = 0$ at a node and so, the mechanical circuit reads intuitively. We can think of force as 'mechanical current' and velocity as 'mechanical voltage'. Fig 2.1 shows a schematic representation of the electromechanical two port model of the transducer, power amplifier and the specimen. The parameter A represents the electrical admittance ($\frac{Current}{Voltage}$) of the transducer when the transducer tip is immobile, represented as an impedance $\frac{1}{A}$ in parallel with a current source B. The parameter D is the mechanical impedance ($\frac{Force}{Velocity}$) of the transducer tip when the voltage across transducer tip is zero and is represented in terms of mobility, $\frac{1}{D}$ in parallel with a force source, C. The parameters B and C are the controlled current or force sources. For some experiments, we will need to include the power amplifier and specimen characteristics as well in the model as illustrated in fig. 2.1. The power amplifier is modeled as a controlled voltage source with gain g and impedance Z_{pa}. The specimen is modeled as a mechanical load with mobility M_s. The complete system model that includes the power amplifier, transducer and the specimen is shown in fig. 2.2. With these definitions, the equations governing the power amplifier-transducer-specimen model are:

$$I_1 = AV_1 + BV_2 \tag{2.1}$$

$$I_2 = CV_1 + DV_2 \tag{2.2}$$

$$V_1 = gV_s - (Z_{pa} + Z)I_1 \tag{2.3}$$

$$I_2 = \frac{1}{M_s}V_2 \tag{2.4}$$

In the above equations, V_1 is the voltage across the tranducer terminals, I_1 is the current in the transducer, V_2 is the output velocity, I_2 is the force on the transducer, V_s is the generated

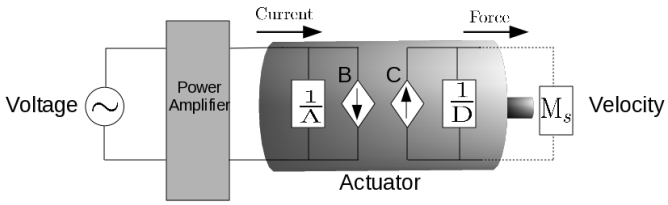

Figure 2.1 Complete electromechanical model of Piezoelectric transducer along with power amplifier and specimen.

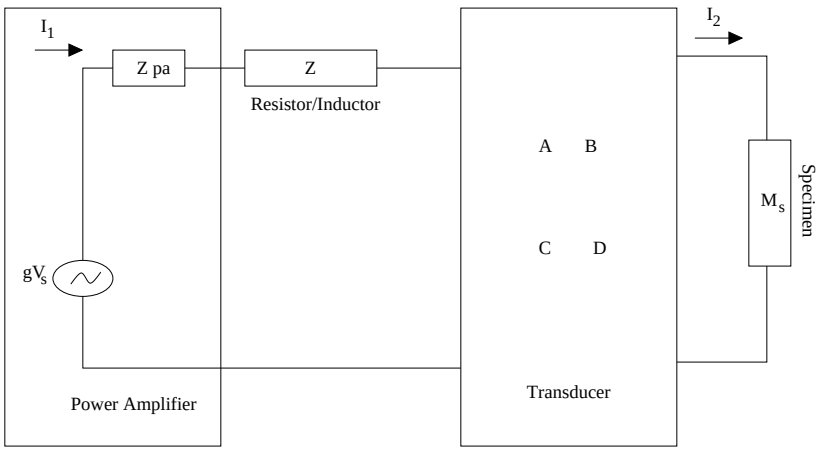

Figure 2.2 Schematic showing all the parameters of the complete Electromechanical model including power amplifier, transducer and specimen.

excitation voltage, Z is the external series resistance (or inductance), M_s is the specimen mobility and A, B, C, D are the four network parameters.

The voltage, V_1 and current, I_1 are measured with the sensors in the system while a laser vibrometer measures the velocity. Therefore V_1, V_2 and I_1 are directly measurable. The transducer force, I_2 is not directly measurable. We will run experiments measuring V_1, I_1 and V_2 in order to evaluate the seven system characteristics: The four transducer parameters A, B, C and D, the two power amplifier parameters g and Z_{pa}, and the specimen mobility, M_s. In order to evaluate these parameters, we performed tests under different external conditions. We added a known mass [1] m (mobility $M_s = \frac{1}{j\omega m}$) in place of the specimen and a known series resistor, R between power amplifier and transducer. With this set up, we excited the transducer with a frequency sweep and measured V_1, V_2 and I_1. We did multiple(6-9) tests with enough combinations of masses and resistors to get an overdetermined system of equations with more equations than unknowns. We solved this system of equations using least squares for the seven system characteristics across the frequency range 3Khz to 25Khz. We used a matched filter denoising algorithm to eliminate the quantization noise from all the measured waveforms. The algorithm is discussed in detail in the appendix.

2.2 Simplified transducer model

The complete electromechanical model solved above depends on seven parameters (power amplifier, two port parameters and specimen) and requires many measurements. We use a simplified equivalent called 'Norton Equivalent circuit' to represent the entire system of power amplifier and transducer[2]. In circuit terminology, a Norton circuit consists of a current source and a parallel source impedance, or in our mechanical model, a force source and a parallel mobility as shown in fig. 2.3(b). This is the simplified representation of the schematic in fig. 2.3(a). Thus, we can define the transducer in terms of any two of the following quantities:

[1] Tungsten blocks were used to approximate point masses in place of specimens for the testing. The high density of tungsten allows it to approximate a point mass better than other materials for higher frequencies.

[2] An equivalent representation, called Thevenin Equivalent circuit consists of a voltage source and a series source impedance

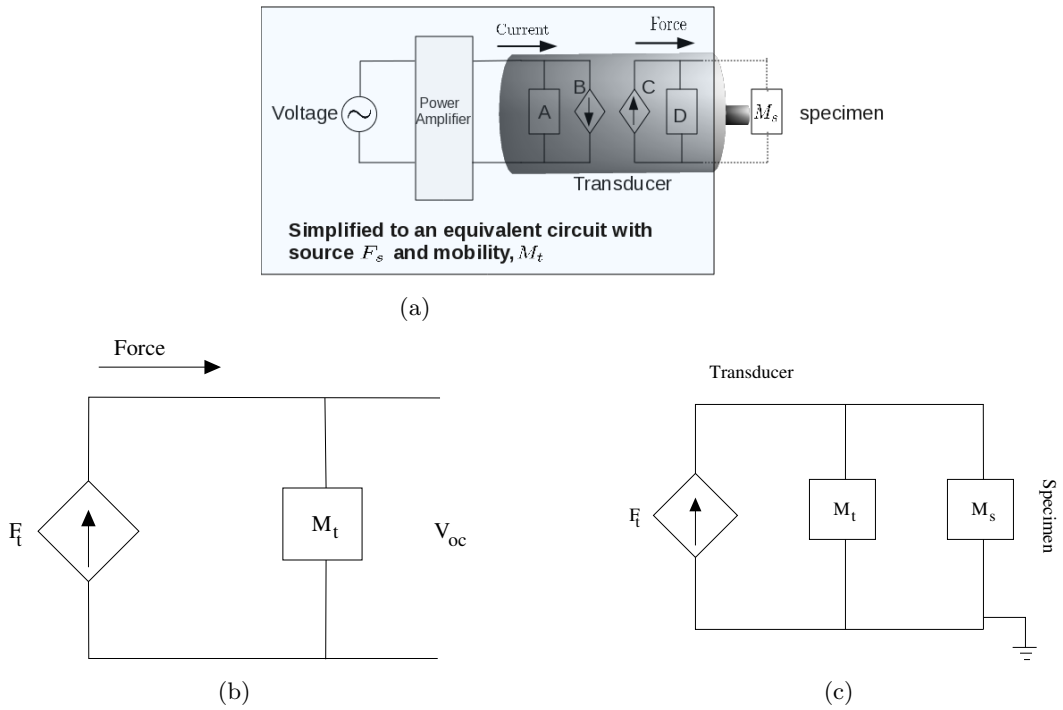

Figure 2.3 Norton equivalent representation of piezo stack transducer with and without a load attached to it. The circuit on the bottom left shows the transducer with no load attached to it, while the one on bottom right shows the transducer with a specimen attached to the tip.

1. *Immovable Object Force (also known as Blocking force)*
2. *Transdcer Mobility*
3. *Transducer Open circuit velocity*

Immovable Object Force, F_t is the force on the transducer tip when an immovable object is attached to it. This is the open circuit velocity divided by the mobility of transducer. It will be calculated by first measuring the open circuit velocity and transducer mobility. The immovable object force is given by: $F_t = \frac{V_{oc}}{M_t}$.

Transducer Mobility, M_t is defined as velocity of the transducer per unit applied force.

The transducer mobility can be calculated using open circuit velocity of transducer and the velocity of a known point mass (in our case, a tungsten block) attached to the transducer tip by applying KCL (Kirchoff's Current Law) along the Norton equivalent cirucit in fig. 2.3(c). The mobility calculated is given by:

$$M_t = \frac{V_{oc}}{(j\omega m)v_m} - \frac{1}{j\omega m} \tag{2.5}$$

where m is the known point mass, V_{oc} is the transducer open circuit velocity, v_m is the velocity of the point mass.

The transducer mobility can also be calculated from the parameters we solved from the model. From fig. 2.2, the transducer mobility, as seen by the specimen with the power amplifier attached and operating is given in equation 2.6.

$$M_t = \frac{V_2}{I_2} = \frac{1}{D - \frac{BCZ_{pa}}{1+AZ_{pa}}} \tag{2.6}$$

Open Circuit Velocity, V_{oc} is the velocity of the transducer tip when no load is attached to it. This is measured by exciting the transducer and pointing a laser vibrometer at the vibrating tip. Since it is easier to measure V_{oc} directly, we used this to calculate transducer mobility and immovable object force. If a Thevenin equivalent is used for the analysis instead, this would be the primary parameter in it (as a velocity source).

Fig. 2.4 shows the plots of mobility and immovable object force of two different transducers calculated from above for different frequencies. The transducer has high open circuit velocity at its resonance frequencies. However, the immovable object force of transducer is relatively flat compared to the rest of the parameters (open circuit velocity, mobility). This is the reason we have decided to model the transducer as a force source.

2.3 Specimen characterization

Specimen characteristics can be easily calculated using the Norton circuit description. When a specimen is attached to the transducer and vibrated, its velocity, v_s is measured using a

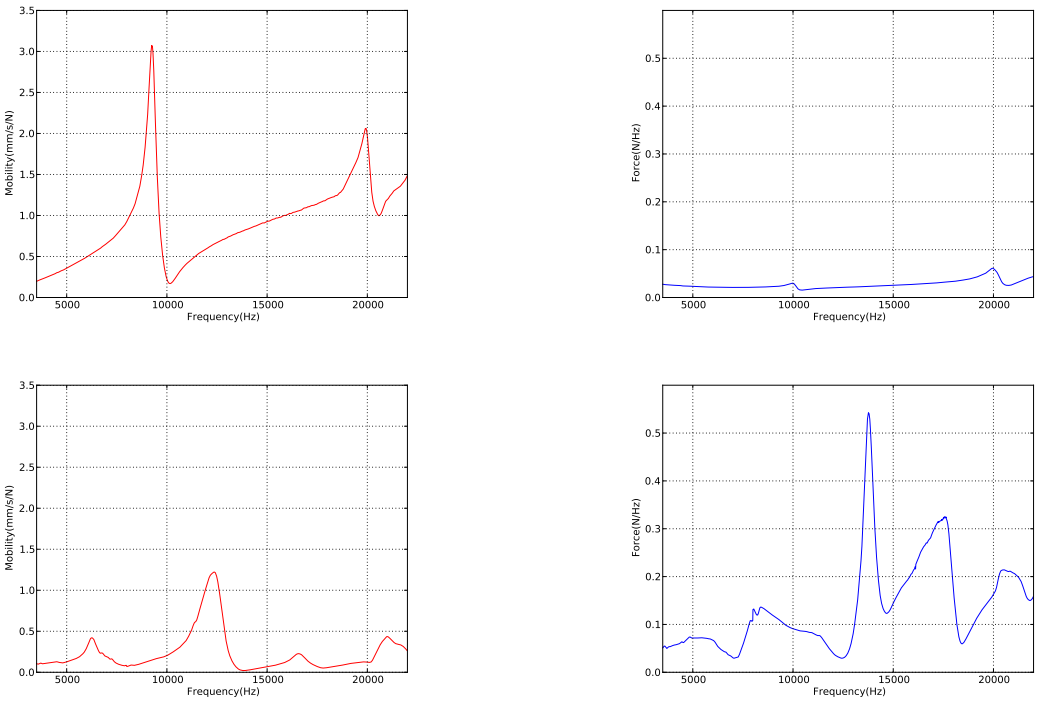

Figure 2.4 Transducer characteristics calculated from the Norton equivalent model. The top left plot shows mobility of the transducer PM1620. The top right plot shows the immovable object force of the same transducer. Bottom left plot shows mobility of the transducer PM2540. The bottom right plot shows the immovable object force of this transducer. The immovable object force of transducers is relatively flat compared to the mobility.

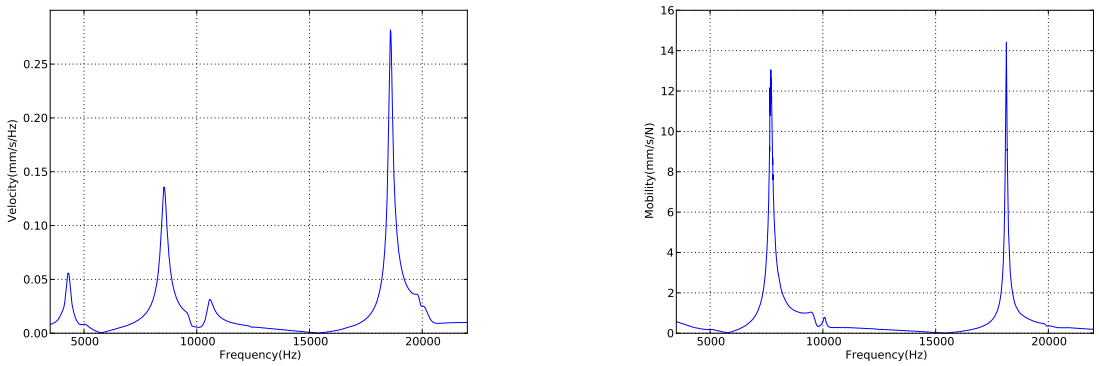

(a) (b)

Figure 2.5 Specimen characteristics calculated from the Norton equivalent model of the transducer with no coupling (metal-metal contact). Plot on the left shows the velocity spectrum of the specimen measured by a Laser Doppler Vibrometer. Plot on the right shows the calculated value of specimen mobility from the model. Clearly, the peaks in velocity profile do not match those in the mobility profile which represent the natural resonances of specimen. This is because of the transducer-specimen system resonances. Adding a couplant breaks these system resonances.

vibrometer. With the previously measured V_{oc} and M_t, the specimen mobility can be calculated from the equivalent circuit by applying KCL (Kirchoff's Current Law) along the circuit of fig 3(c), i.e., by solving equation 2.7 and using the fact that $F_t M_t = V_{oc}$,

$$v_s = F_t \frac{M_t M_s}{M_t + M_s} = V_{oc} \frac{M_s}{M_t + M_s} \tag{2.7}$$

The specimen mobility is calculated using equation 2.7 as $M_s = \frac{M_t V_s}{V_{oc} - V_s}$. The plots of velocity and mobility for a rectangular bar specimen, with no coupling medium are shown in fig. 2.5. Figure 2.5(a) shows the measured specimen velocity and 2.5(b) shows the specimen mobility calculated form velocity and transducer characteristics. The mobility peaks are the natural resonances of the specimen. Note that the natural resonances seen in fig. 2.5(b) do not line up with the velocity peaks in fig. 2.5(a). The velocity peaks (maximum measured motion) are observed not at the specimen resonant frequencies, but instead at other frequencies that are resonances of the **transducer-specimen system**. This is because the specimen and transducer interact to form combined system resonances which are different with each transducer. Depend-

ing on which transducer is used, the specimen velocities vary greatly. The system resonances also depend very strongly on details of mounting. So as to make a repeatable measurement, it is extremely critical to disconnect the specimen resonances from the system resonances. We have observed that adding a coupling medium breaks these system resonances and makes the specimen vibrate at its natural resonances.

2.4 Couplant behavior and characterization

In vibrothermography, a couplant is often used between transducer tip and specimen. The reason for this has not been completely understood to date, except that practitioners have discovered that couplant made tests more reproducible and reduced the risk of surface damage to the specimen. Common choices for couplant are layers of card stock, teflon tape, paper and plastic sheet. As discussed above, when we use a layer of card stock as couplant between transducer tip and specimen, it breaks the system resonances, so the specimen vibrates at its own natural resonances and not at system resonances.

This effect is better demonstrated in fig. 2.6. Figures 2.6(a) and 2.6(b) show specimen velocities using different transducers with and without a couplant respectively. The spectra are similar and the resonant frequencies are almost identical for all transducers when a couplant is used. Without a couplant, in the spectra of fig. 2.6(b), the resonant frequencies are all completely different. From these figures, it is clear that using a couplant eliminates the system resonances.

To model the effect of couplant, We modified the Norton model to represent the couplant as an elastic spring (stiffness k_c) between transducer tip and specimen. The mobility of the spring is $\frac{j\omega}{k_c}$[13]. This modified Norton circuit is shown in fig. 2.7. The specimen mobility, calculated by applying KCL (Kirchoff's Current Law) in the circuit of fig. 2.7 is $M_s = \frac{v_s(M_t+M_s+\frac{j\omega}{k_c})}{F_t M_t}$. Using this mobility and the fact that $F_t M_t = V_{oc}$, the specimen velocity, v_s is calculated as:

$$v_s = \frac{V_{oc} M_s}{M_t + M_s + \frac{j\omega}{k}} \tag{2.8}$$

The resonances occur when the denominator in equation 2.8 approaches zero. In this equation, the transducer and specimen mobilities M_t and M_s are complex and possibly negative

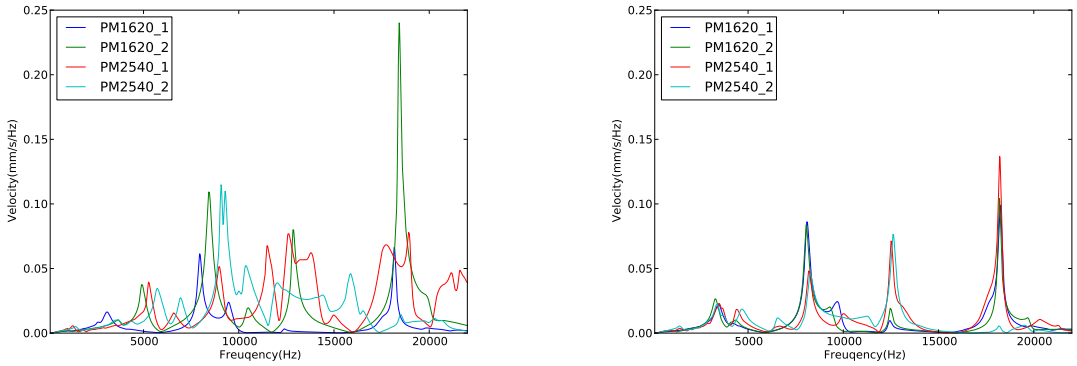

(a)

(b)

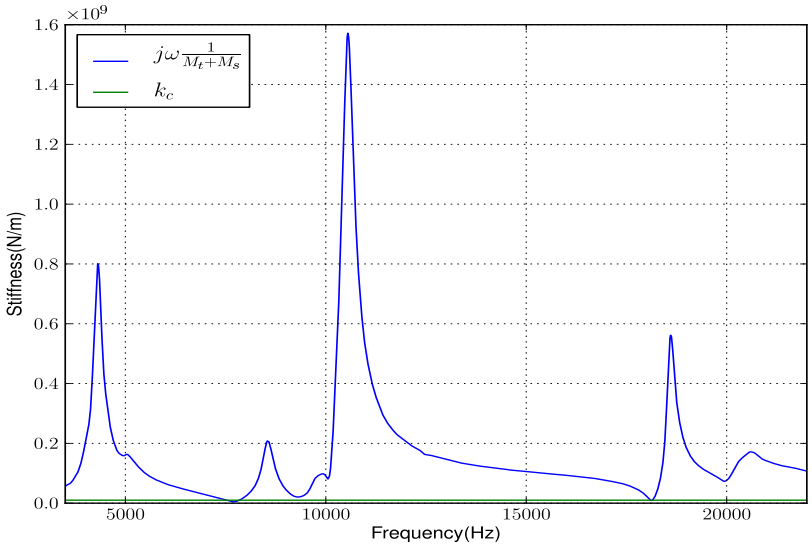

(c)

Figure 2.6 Effect of adding a couplant on specimen behavior. The top left plots show the velocity response of a rectangular bar specimen with four different transducers with metal-metal contact. The resonances in the specimen velocity are not repeatable. The top right plots show the same but with a couplant in between transducer tip and the specimen. In this case, the system resonances are broken and we only see the specimen resonances which are very repeatable across transducers. The plot on the bottom shows the reason for this behavior. If the compliance of the couplant is small enough to dominate, the system resonances are eliminated.

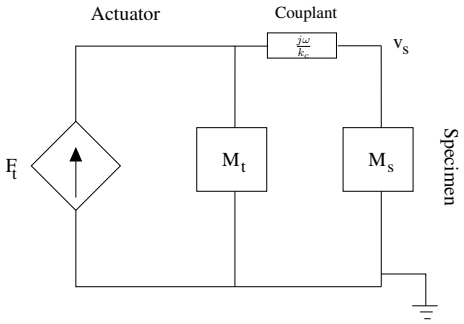

Figure 2.7 Norton equivalent mechanical model of transducer with specimen attached as the load with a couplant between transducer tip and specimen. The couplant, in this context acts like a spring whose electromechanical analogue is an inductor.

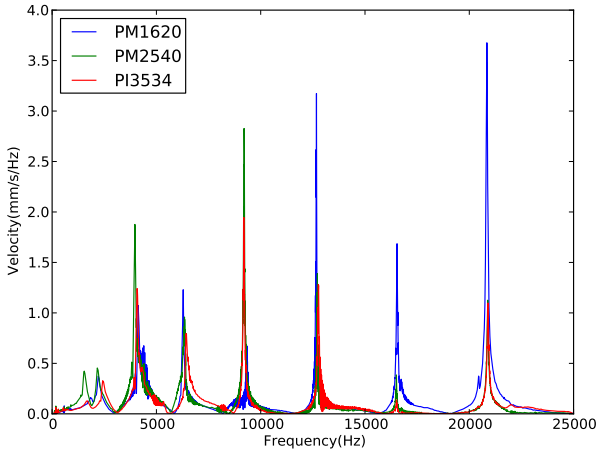

Figure 2.8 Velocity spectra of a rectangular bar specimen measured at high amplitude excitation using three different transducers and one layer of card stock as a couplant. The peaks in velocity spectrum are all identical irrespective of the transducer used. This demonstrates the fact that using a couplant breaks system resonances even at high amplitude excitations.

while the couplant stiffness $\frac{j\omega}{k}$ is always positive imaginary. So, the system resonances are effectively eliminated when $\frac{j\omega}{k_c}$ is so big that it dominates M_s and M_t:

$$\frac{j\omega}{k_c} \gg M_s + M_t$$

or equivalently,

$$k_c \ll \frac{j\omega}{M_t + M_s} \tag{2.9}$$

The physical meaning of the condition in equation 2.9 is that a sufficiently compliant couplant completely separates the system resonances from the specimen resonances. When this happens, the specimen velocity can be approximated from equation 2.8 by:

$$v_s \approx \frac{k_c}{j\omega} V_{oc} M_s \tag{2.10}$$

When the condition in equation 2.9 holds, the specimen velocity depends on the product of transducer open circuit velocity and specimen mobility and not on the combined mobility of specimen and transducer $(M_s + M_t)$. In the plot shown in fig. 2.6(c), the horizontal line in green shows the stiffness of the couplant we used. For the case of a single layer of card stock couplant we used for this test, the k_c from static measurement was found to be approximately 10000 KN/m. From this plot, we verified that the condition in equation 2.9 indeed holds for the experiment shown in figures 2.6(a) and 2.6(b). The couplant compliance can be increased by increasing the thickness of the stock. However, specimen velocity decreases as couplant becomes more compliant. Hence, a couplant whose compliance is just small enough to eliminate the system resonances but does not heavily damp the specimen motion is ideal to use in vibrothermography.

We have also observed that at high amplitude excitation where the system is not completely linear, the couplant still breaks the system resonances. Plots in fig. 2.8 show the velocity spectra of a rectangular bar specimen when excited at high amplitude frequency sweep. The velocity peaks in the spectra are the same irrespective of the transducer used. This clearly illustrates that adding a couplant breaks the system resonances and makes the test more repeatable.

2.5 Transducer selection criteria

The key parameter for transducer selection is transducer open circuit velocity, V_{oc}. This is because, with a couplant, the specimen velocity, $v_s \approx (\frac{k_c}{j\omega} M_s) V_{oc}$ and is therefore proportional to V_{oc}. A transducer with large open circuit velocities at or near the specimen resonances gives maximum specimen motion(v_s). The ideal choice for a transducer would be to use one with flat open circuit velocity spectrum. However, transducer velocity has its own natural resonances and nulls in response as well. These resonances depend on the geometry of the piezo stack inside the tranducer, and vary even between nominally identical transducers as shown in fig. 2.9. Transducers with longer piezo stacks generally have lower main resonance frequencies. Transducers with large diameter piezo stacks are stiffer (i.e., lower M_t) because the larger cross sectional area gives more volume of piezo stack to deform. In part because of their higher capacitance, the source velocity of large diameter stacks is generally lower than small diameter piezo stack transducers for the same excitation amplitude.

To see the variation of open circuit velocity with stack geometry, we calculated the Norton parameters of all ten transducers and grouped them based on their stack diameters of 16, 25 and 35mm with lengths of 20, 40 and 60 mm each. We then plotted all these three sets of velocities in fig. 2.9. The open circuit velocities (V_{oc}) of large diameter stack transducers are much smaller than the small diameter ones but they are more uniform in frequency. Apart from this, however, we could not conclude much from these plots.

2.6 Techniques to flatten transducer velocity

As can be seen in fig. 2.9, the transducer open circuit velocity is not uniform at all frequencies. With a uniform V_{oc}, the dependence of specimen motion on transducer velocity decreases (equation 2.10) and test becomes independent of the transducer used. To flatten the velocity response, we have to compensate for the effect of transducer resonances on the spectrum. Since the mechanical resonances are determined by transducer geometry, these cannot be directly modified except by changing geometry. Aside from the design difficulties, such a technique would tend to shift the resonant frequencies, not eliminate or dampen them. In contrast, elec-

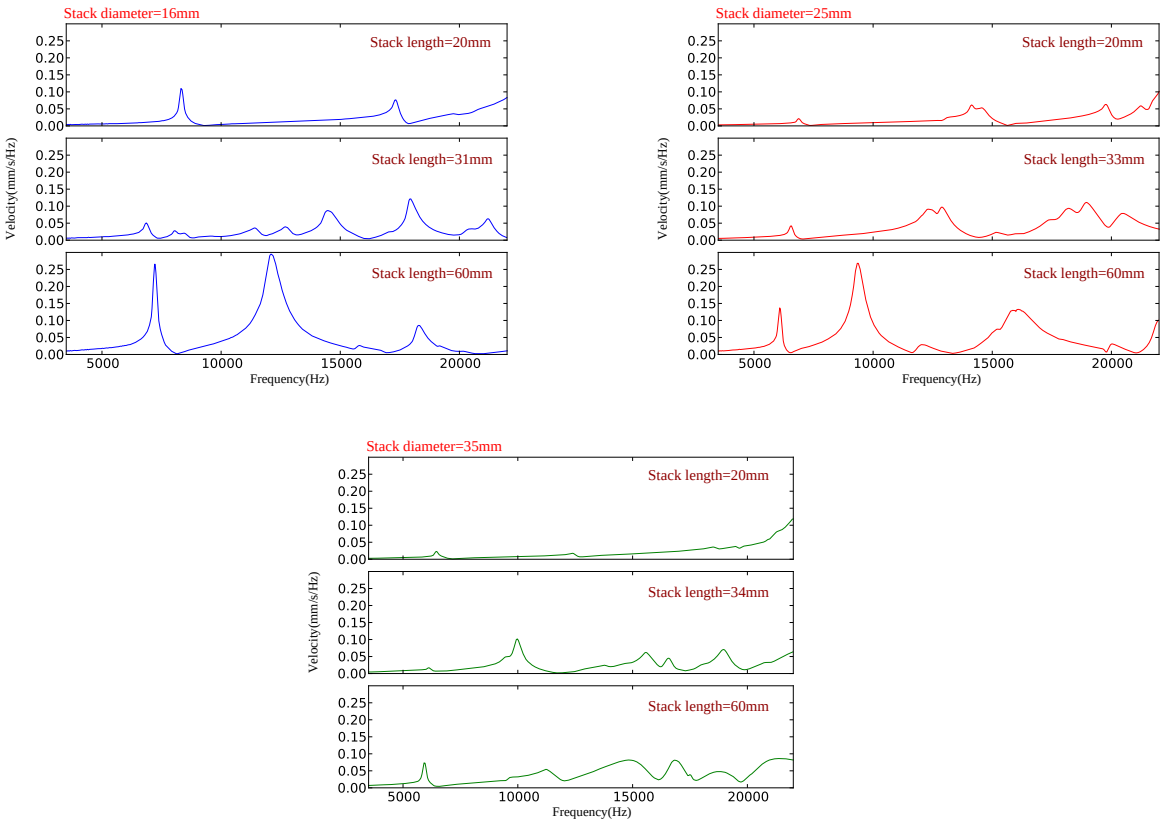

Figure 2.9 Source velocity, V_{oc} plots of all different transducers with our McIntosh power amplifier ($Z_{pa} \approx 3\Omega$ and g = -180). Transducers of same stack diameter and lengths of 20, 40 and 60mm are grouped together. The transducers on top left have 16mm diameter while the ones on right and bottom plots have 25mm and 35mm respectively.

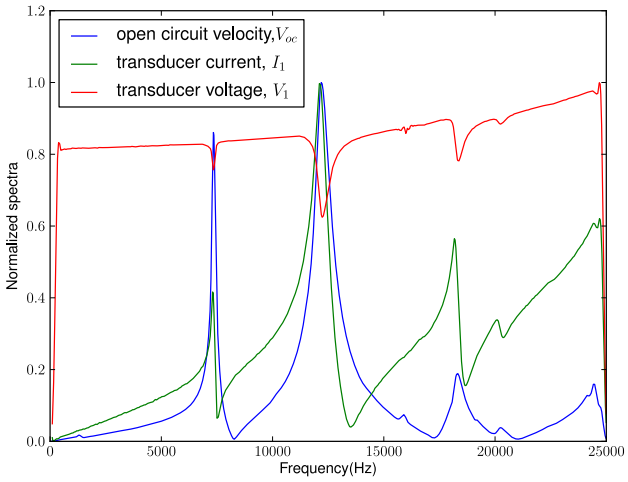

Figure 2.10 Normalized velocity, current and voltage of the transducer PM1660 with a frequency sweep excitation. The plot in blue shows the normalized transducer velocity, the plot in green shows the normalized current and the plot in red shows the normalized transducer voltage. These plots demonstrate that the transducer open circuit velocity is correlated with the current and not voltage and that adding electrical resonances helps flatten the velocity.

trical behavior can be adjusted by adding passive components such as an inductor. When the transducer is excited with a frequency sweep, we observed that the transducer open circuit velocity correlates primarily with the current as opposed to transducer voltage as illustrated in fig. 2.10. The plot in blue shows the normalized open circuit velocity of transducer, the plot in green shows the normalized current and the plot in red shows the voltage for the transducer PM1660. The correlation between velocity and current is true for all other transducers tested. So, a modified current might result in an improved flatter velocity spectrum. We attempted to do this in two ways:

1. by introducing electrical resonances and
2. by changing the voltage excitation waveform to get a flatter source velocity.

2.6.1 Introducing electrical resonances with an inductor

An electrical resonance can be created by adding an inductor (inductance L) in series with the transducer. The inductor, combined with the inherent capacitance of the transducer forms an " LC tank circuit "[14]. This schematic is shown in fig. 2.2 where energy resonates between magnetic storage in the inductor and electrical storage in the capacitance of the transducer. The resonance frequency, f_r is given by:

$$f_r = \frac{1}{2\pi\sqrt{LC_t}} \tag{2.11}$$

In equation 2.11, C_t can be estimated from a frequency domain curve fit of the quantity $\frac{V_1}{I_1} = \frac{1}{j\omega C_t}$, V_1 and I_1 are the voltage and current in the transducer measured electrically. For a known C_t and required resonance frequency f_r, the value of L can be calculated using equation 2.11. In this case, we added a 1.6mH air core toroidal inductor to the transducer PM3520 (C_t = 835nF) to generate an electrical resonance at around 14Khz. The inductance of an air core toroidal inductor of cross section area A_{cs} and mean radius R is given by[15] :

$$L = \frac{\mu_0 N^2 A_{cs}}{2\pi R} \tag{2.12}$$

The number of turns to achieve this inductance is calculated from:

$$N = \sqrt{\frac{L2\pi R}{\mu_0 A_{cs}}} \tag{2.13}$$

The wire gauge of copper winding should be chosen so that the internal resistance of coil is negligible compared to the electrical impedances of power amplifier and transducer. Fig. 2.11 shows how the added inductor helps to flatten the open circuit velocity (V_{oc}). The plot in blue shows the transducer velocity without inductor and the plot in green shows the same with the inductor added in series. The transducer has a mechanical resonance at around 22Khz. The inductance was chosen to generate an electrical resonance at around 14Khz so that the combined velocity gets increased around 14 Khz(electrical resonance) and attenuated at 22 Khz (mechanical resonance), giving a flatter V_{oc}. The reason to use aircore inductors is because they are linear and do not saturate unlike ferrite core inductors. For the plots in fig. 2.11, we used a 1.6mH air core toroidal inductor of 550 turns using an AWG 19 copper wire.

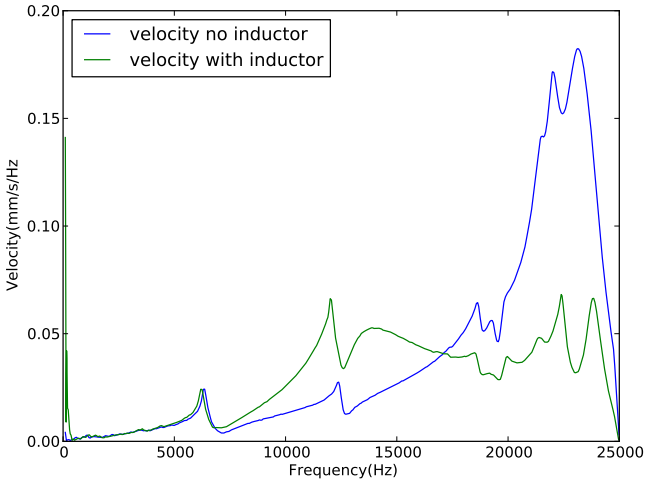

Figure 2.11 Velocity spectrum of the transducer PM3520 for excitation with and without an inductor. The plot in blue shows the transducer velocity without an inductor and the plot in green shows the same with an inductor in series. Adding an inductor in series generates an electrical resonance that compensates for mechanical resonance and flattens the overall response.

Adding an inductor increases the transducer voltage near the electrical resonance frequency. It can even push the transducer voltage well beyond the output voltage of the power amp, as shown in fig. 2.12. The transducer voltage at 14 Khz with inductor is much higher than without the inductor. Since the transducer is specified to operate in 0-1000V or -200 to 1000V, one should be careful not to exceed these limits while adding inductor to the system.

For a transducer with small stack length and large stack diameter, the mechanical resonances are at high frequencies. By choosing an appropriate inductor as we did for fig. 2.11, it is possible to create an electrical resonance at a slightly lower frequency than the mechanical resonance to make the spectrum more uniform through a large frequency range. So, transducers with this stack geometry can be used effectively for a large range of high frequency inspections. So we recommend large diameter and shorter piezo stack transducers (such as PM3520) for higher frequency work and large diameter, and longer stack transducers (such as PM3560) for low frequency work, when combined with the proposed alternative amplifier discussed in the sections that follow.

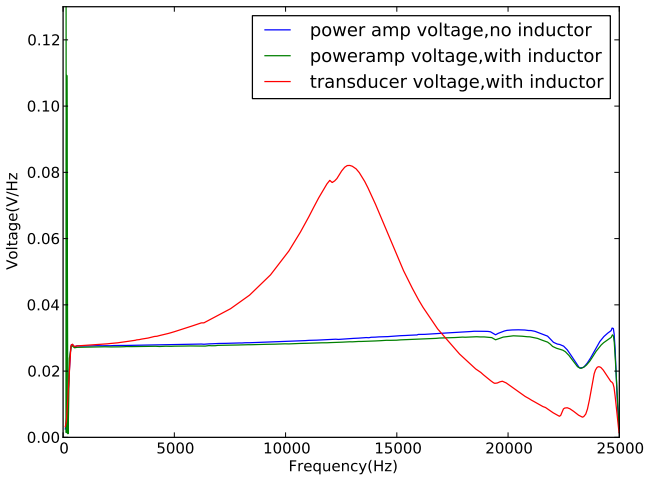

Figure 2.12 Voltage across the transdudcer PM3520 for excitation with and without an inductor. The plot in blue shows the power amplifier output voltage without an inductor, the plot in green shows the same when an inductor is added in series, and the plot in red shows the transducer voltage for the case of a series inductor. Note that when there is no inductor present, the power amplifier voltage and transducer voltage are the same.

2.6.2 Customizing the excitation waveform

Our other approach to flatten the transducer velocity is to predetermine the desired open circuit velocity (V_{oc}) in frequency domain and then calculate the voltage excitation waveform (V_s) that generates this velocity from the model. In the circuit of fig. 2.2, when there is no specimen attached and no external resistor (or inductor) is present, the force on transducer tip, I_2=0, velocity $V_2 = V_{oc}$ and Z=0.

The transducer two port equations (eqns 2.1 and 2.2) are then modified and written in matrix form as follows:

$$V_{oc}\begin{bmatrix} B \\ D \end{bmatrix} = \begin{bmatrix} 1 & -A \\ \frac{I_2}{I_1} = 0 & -C \end{bmatrix}\begin{bmatrix} I_1 \\ V_1 \end{bmatrix} \tag{2.14}$$

We calculate the excitation voltage, v_s that generates the desired V_{oc} in frequency. Unfortunately, for this calculation we need the values of the parameters A, B, C and D. However, instead of having to do multiple tests (as discussed in the section 2.1), the parameters A, B, C, D

for this calculation can be estimated in a simpler way with two tests if the characteristics of power amplifier (g and z_{pa}) are known: One with a specimen of known mobility attached to the transducer (current I_1=I_{11}, voltage V_1=V_{11}, specimen velocity V_2=v_m) and the other without a specimen attached (current I_1=I_{11}, voltage V_1=V_{11}, tip velocity V_2=V_{oc}^{meas}). The transducer mobility, M_t is calculated from the data collected in these tests using equation 2.5. The other parameters are then calculated as:

$$\begin{aligned} D &= \frac{1}{M_t} \\ C &= -D\frac{V_{oc}^{meas}}{V_{11}} \\ A &= \frac{I_{11}}{V_{11}} \\ B &\approx -C \end{aligned} \tag{2.15}$$

Once the parameters are calculated, the excitation voltage waveform that generates the required V_{oc} is given by:

$$V_s = \frac{1}{g}\begin{bmatrix} Z_{pa} & 1 \end{bmatrix}\begin{bmatrix} 1 & -A \\ 0 & C \end{bmatrix}^{-1}\begin{bmatrix} B \\ -D \end{bmatrix} V_{oc} \tag{2.16}$$

When an inductor (inductance L) is included in the circuit of fig. 2.2, the external impedance Z is equal to $j\omega L$ instead of zero and the simulated excitation voltage becomes

$$V_s = \frac{1}{g}\begin{bmatrix} Z_{pa} + j\omega L & 1 \end{bmatrix}\begin{bmatrix} 1 & -A \\ 0 & C \end{bmatrix}^{-1}\begin{bmatrix} B \\ -D \end{bmatrix} V_2 \tag{2.17}$$

These techniques can help flatten the velocity spectrum, but the resonant behavior of transducer is inherent and cannot be completely eliminated without unreasonably limiting the output velocity.

CHAPTER 3. HIGH AMPLITUDE BEHAVIOR OF TRANSDUCER

So far, the emphasis has been on the small signal analysis of the transducer. However, real life vibrothermography tests are performed at much higher amplitudes so as to provide enough energy to generate detectable heating. So, we extend our analysis to include the effect of high amplitude excitation on transducer and power amplifier behavior. At high amplitude excitation, the system is limited by the power amplifier. Commonly used transistor based power amplifiers are constrained by the voltage limits defined by the breakdown voltage of Si (about 200V). In these power amplifiers, once the maximum gain limit is reached, the amplified signal gets clipped and the higher order harmonics dominate the spectum. Our MC1201 power amplifier, on the other hand has a protective circuit called 'power guard' that turns down the gain once a threshold for current is occurred and this makes it a current limiting power amplifier. It has a huge volume of output transformers that allow it to generate higher voltages. The MC1201 is expensive for this reason.

3.1 Effect of power amplifier saturation

At low excitation amplitude, the current flow in the system is small and no constraints regarding power amplifier or transducer are imposed on the system. Our McIntosh power amplifier seems to limit the current at approximately 9A maximum independent of voltage. As the excitation voltage increases from low to high amplitudes, so does the current flow. Once the threshold limit of 9A is reached, increasing the excitation voltage does not affect the current because a protection circuit called 'power guard' turns down the gain and prevents further increase in the current. Transducers whose piezo stacks have diameter and longer length (eg: PM3560) have larger capacitance and stiffness compared to transducers with smaller volume

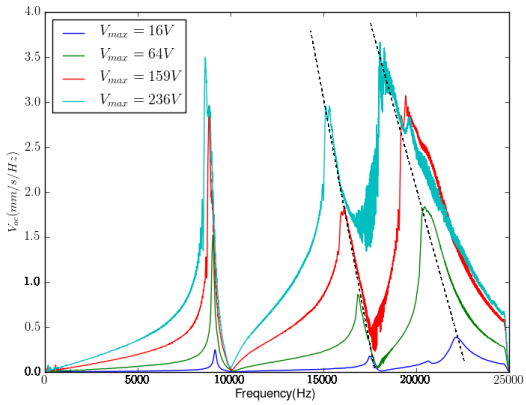

Figure 3.1 Open circuit velocity of the transducer PM1620 for different excitation voltages. As the excitation voltage increases, the higher order resonances shift towards lower frequencies as shown by the dotted lines. The legend in the figure shows the maximum AC voltage applied across the transducer. At the 236V excitation voltage, the magnitude of harmonics is comparable to that of the fundamental, which as a result distorts the spectrum.

stacks. Due to this reason, large amounts of current are required to generate motion in these transducers. As a result, the current threshold often occurs before the stacks achieve desired velocity (and therefore dynamic stresses) for defect detection.

As the excitation amplitude increases, the inherent non linearity of PZT starts to dominate the transducer behavior[16]. As a result of this, the higher order transducer resonances steadily shift towards lower frequencies and harmonics start increasing in amplitude. This phenomenon is shown in fig. 3.1.

Since the transducer velocity primarily correlates with current, and the current in the transducer cannot be further increased after saturation occurs, the velocity does not increase either. Fig. 3.2 illustrates the saturation behavior of the power amplifier for two different input voltages (fig 3.2(a) is at 0.8V and fig. 3.2(b) at 1.8V). As the power amplifier saturates, the protection circuit turns down the gain so that the current does not exceed its maximum value. Unfortunately, this current saturation effect nullifies the possible benefit of adding an inductor. This is because at an electrical resonance, the current in the transducer becomes large, immediately saturating the power amplifier.

We expect that with a power amplifier that is not strictly current limited, or by using a

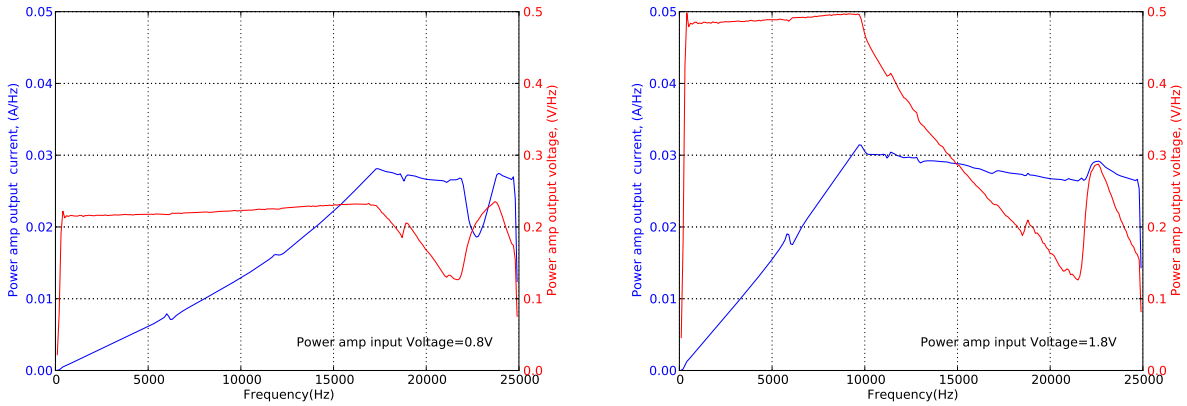

(a) (b)

Figure 3.2 Frequency spectra of current and voltage across the transducer PM2530 when power amplifier saturates for different input voltages. The plots in blue show transducer current and the plots in red show transducer voltage. The power amplifier input voltage is 0.8V for the plots on left and 1.8V for the plots on the right. The maximum magnitude in the current specta of both plots is same despite a much higher input voltage in the figure on right.

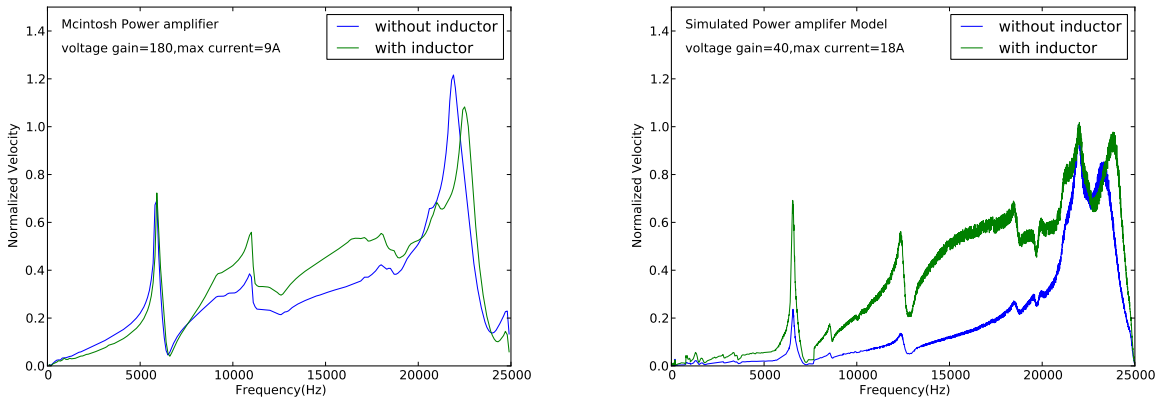

(a) (b)

Figure 3.3 Comparison of normalized transducer open circuit velocity V_{oc}, with and without an inductor when using a transformer-less power amplifier and our McIntosh MC1201 power amplifier. The plots on the left show the measured transducer velocity using our McIntosh power amplifier for the transducer PM3520 and the plots on right show the simulated velocity using a transformer-less power amplifier. We hypothesize that using a transformer-less power amplifier might help flatten the transducer open circuit velocity.

current amplifier instead of a voltage amplifier, there would be an improvement by adding an inductor. We hypothesize the use of a high voltage transformer-less power amplifier such as Yamaha T5n, which is rated to drive a 2Ω load over 20Hz-20KHz and predict its performance based on our model. Fig. 3.3 compares the transducer open circuit velocity using the hypothesized model and our MC1201 power amplifier. The plots in fig. 3.3(a) show measured velocity using our MC1201 power amplifier. The plots in fig. 3.3(b) show simulated velocity using a transformer-less power amplifier. With a power amplifier that has no current saturation issues, adding an inductor will make the spectrum of short piezo stack transducers more uniform over a frequency range from 10KHz-25KHz. We would expect similar broad uniformity over lower frequencies for longer piezo stack transducers.

3.2 Transducer degradation

In our experience using broadband transducers for vibrothermography, we have noticed that the stress levels achieved with a transducer that has been in service seem to degrade over time and usage. To investigate the long term reliability of the broadband piezo stack transducers, we tried to analyze the useful life of the transducer. For this study, we used an off the shelf PI2533 transducer and tested its long term behavior at high amplitudes. We excited the transducer with a 10KHz sinusoidal input with a peak to peak voltage of 350V with no specimen attached and monitored the open circuit velocity at each trigger. The transducer was allowed to cool between successive triggers so that the effect of the piezo stack heating up (due to successive high amplitude excitations) on the test is minimized. To keep track of how the overall spectrum of transducer changes as it degrades, we excited the transducer with a low amplitude frequency sweep (from 100 Hz to 20 Khz at 17V peak to peak voltage) periodically after every 10 bursts and a high amplitude frequency sweep (from 100 Hz to 20 Khz at 175V peak to peak voltage) after every 100 low amplitude sweeps[1]. The excitation voltages for the high amplitude tests are chosen so that they are close to the normal voltage levels required for vibrothermographic testing without saturating the power amplifier. The transducer velocity, current and voltage

[1]Note that the peak to peak voltages are centered about the 500V external DC voltage provided by the bias generator

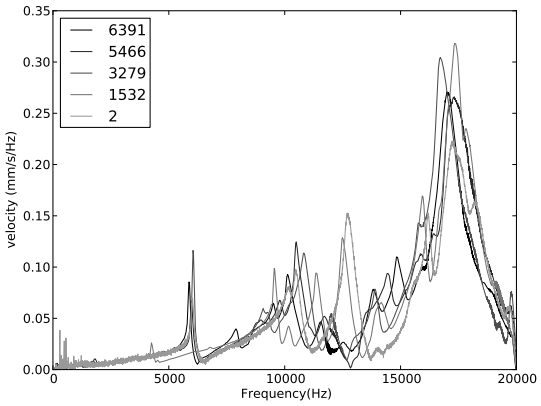

Figure 3.4 Small signal spectrum of the transducer PI2533 after 2, 1532, 3279, 5466 and 6391 triggers in increasing order of grayscale. The higher resonance frequencies are shifted across the triggers, but the magnitude of the spectrum did not change significantly.

waveforms of all the tests were separately saved for each type of excitation for post processing. All the tests were automated by a python script that issued commands to dataguzzler from within the script and saves the data after each trigger. The test was stopped after a total of 6397 triggers (5800 tone bursts, 585 low amplitude sweeps and 12 high amplitude sweeps).

The data sets for burst excitation, low amplitude sweep and high amplitude sweep were analyzed separately. The velocity spectrum for all the sweep tests has been calculated from the data. Fig. 3.4 shows the magnitude of low amplitude spectrum of the transducer at various stages of testing. The spectrum of the tranducer remained almost unchanged upto a frequency of about 8 Khz. At frequencies above 8 Khz, even though the magnitude of the spectrum did not follow a clear trend, the resonance frequencies have shifted across all the 6400 triggers.

Fig. 3.5(a) shows the plots of the transducer high amplitude spectrum as the test progressed. Unlike the small signal spectrum, in the high amplitude spectrum, there is intereference between the fundamental component and higher order harmonics because of which the spectrum does not look as clean as the low amplitude spectrum. To overcome this interference effect, we separated the harmonics and the fundamental component using a matched filter algorithm and plotted them separately as shown in fig. 3.5. The filtering method is discussed in detail in appendix. Fig. 3.5(a) shows the raw spectrum of the transducer as calculated from the Fourier

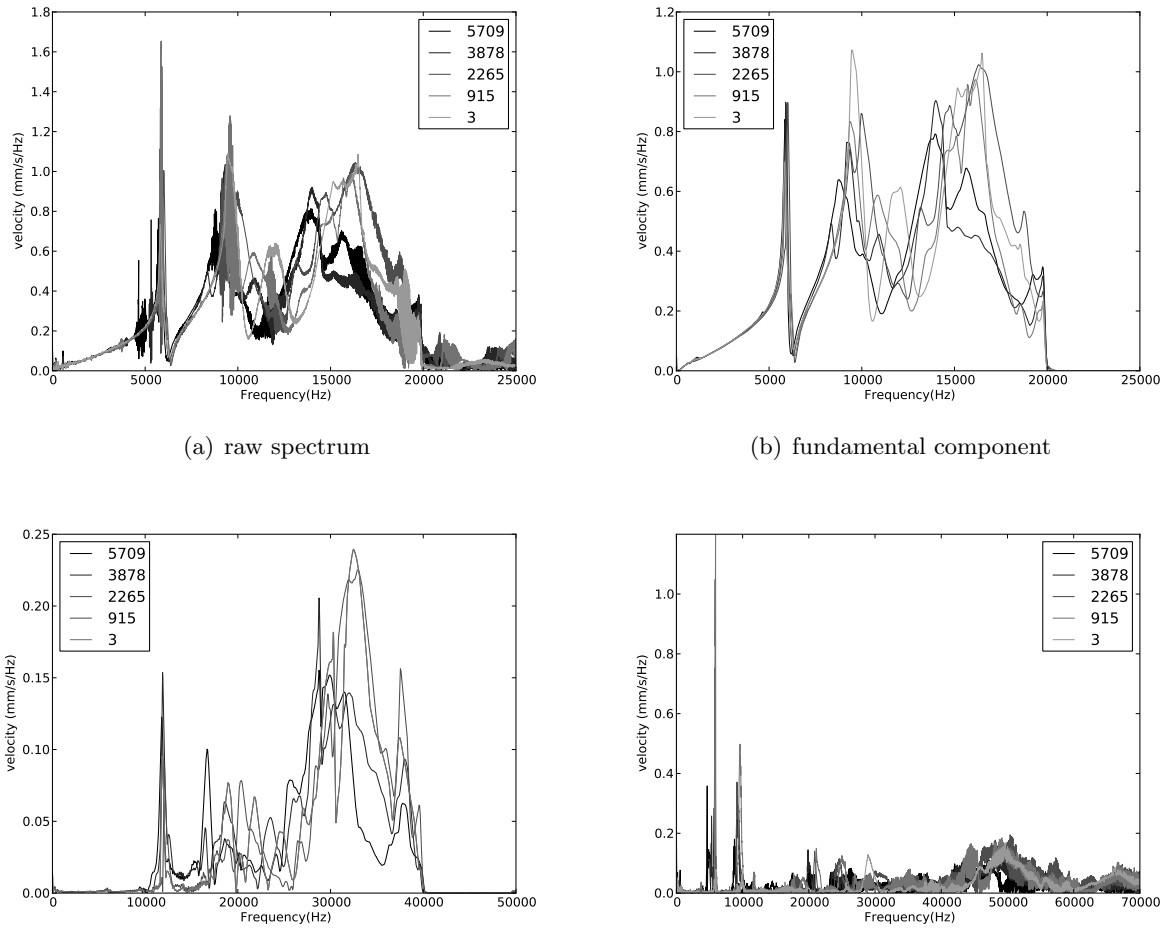

(a) raw spectrum

(b) fundamental component

(c) second harmonic

(d) residuals

Figure 3.5 High amplitude spectrum of the transducer PI2533 calculated after 3, 915, 2265, 3878 and 5709 triggers with decreasing gray scale levels. The plot on the top left shows the complete raw spectrum without any filtering. The plot on top right shows the fundamental component of the spectrum and the plot on bottom left shows the 2nd harmonic. The plot on bottom right shows the residuals after subtracting the fundamental and second harmonic from the raw spectrum. Legend shows the trigger number of the corresponding test. Unlike the small signal spectrum, the high amplitude spectrum has changed considerably across the triggers.

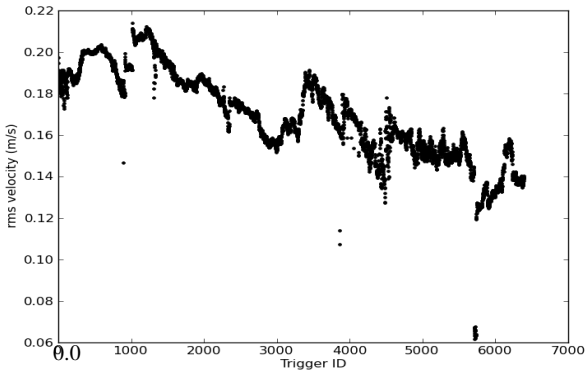

Figure 3.6 rms value of velocity of all the tone burst excitations of the tranducer PI2533.

Transform without any filtering. Figs. 3.5(b) and 3.5(c) show the fundamental and 2^{nd} harmonics of the spectrum respectively. Fig. 3.5(d) shows the residual obtained after subtracting the fundamental and 2nd harmonic from the original spectrum. This contains various higher order harmonics and sub-harmonics that were filtered out. The fundamental component of the spectrum remained almost unchanged upto about 8 Khz. At higher frequencies, however, the spectrum magnitude has changed siginificantly across all the 6400 triggers. This conclusion was not obvious in the raw spectrum because of the interference between fundamental and harmonic components. Even the resonance frequencies have shifted considerably. Some of the originally wider high frequency resonance peaks started to shrink in width and the higher order resonance frequencies shifted towards lower frequencies with more triggers. We hypothesize that this might be an indication of the piezo stack degrading, because when the stack degrades, its stiffness changes and therefore the resonances change too. Note that the change in spectrum across the triggers is purely a transducer phenomenon (and not a result of power amplifier possibly saturating) as the test was performed under the threshold limits of power amplifier.

As a second verification for the above trend, the root mean square (RMS) value of the velocity waveforms for burst excitation was calculated as a measure of the velocity amplitude. This value is plotted with the trigger ID as shown in fig. 3.6. From the plot, one can conclude that in general, the overall RMS value of the velocity decreases over the 6400 triggers. The fact that the resonance frequencies shifted around as the test progressed (as seen in fig. 3.5(a)) might

be an explanation for the local variations in the velocity. The outlier in the data at trigger number 900 was caused by a sensing failure in laser vibrometer. We were not able to come to a meaningful conclusion regarding the outliers at trigger number 3800 and 5800. However, they seem to occur right after a high amplitude sweep test is performed. So, we hypothesize that the hysteresis generated by switching from high frequency sweep to low frequency sweep could be related. Some conclusions for this particular transducer made from this study are given in table 3.1:

Table 3.1 Conclusions from the high amplitude life time testing of transducer PI2533 across all the 6400 triggers

	Low frequency(upto 8Khz)	**High frequency(above 8Khz)**
Small signal	transducer behavior remained mostly unchanged	resonance frequencies shifted but magnitude did not change significantly
High amplitude	transducer behavior remained mostly unchanged, although the lowest order resonance shifted slightly	spectrum magnitude decreased and resonances shifted towards lower frequencies

CHAPTER 4. CONCLUSION

In this study, we modeled the excitation system for vibrothermography including power amplifier, transducer and specimen. Using this model, we addressed questions such as how to select transducers for vibrothermography, transducer-specimen interaction, how using a couplant can break non-repeatable system resonances, type of power amplifier to use and the techniques to flatten the transducer velocity spectrum.

The three important characteristics of a transducer are its open circuit velocity, mobility and immovable object force. The key transducer parameter that governs the specimen behavior is transducer open circuit velocity, V_{oc}. The specimen motion is proportional to the transducer's open circuit velocity when the coupling between them is compliant enough. So, it is desirable to choose a transducer with flatter velocity spectrum so as to reduce the dependence of the specimen motion on transducer being used. Transducers with larger diameters have relatively flatter velocity spectra as compared to that of smaller diameter transducers. From our analysis, the geometry of PM3520 is the best balance between flatness, output velocity and power handling capability, especially when combined with an inductor and high voltage transformerless power amplifier. An additional advantage of large transducers is that despite the high cost, they are inherently more robust. However, with a current limited power amplifier, transducers with huge volume of piezo stacks such as PM3560 have high capacitance and make the power amplifier saturate before the desired vibrational levels have reached. We hypothesized the use of a high voltage transformer-less power amplifier such as Yamaha T5n and used it in our model to predict its performance at high amplitude excitation. We predicted that there would be an improvement in the transducer performance when this type of power amplifier is used with an inductor in series with the transducer. At high amplitude excitation, the transducer behavior becomes increasingly non linear and the higher order resonance frequencies gradually

shift to the left. We observed that the velocity spectrum of transducer changes considerably as the piezo stack degrades. Even though the low amplitude behavior does not change significantly, the high amplitude spectrum decreases in magnitude as the transducer wears. At high amplitudes, the interference of higher order harmonics with the fundamental component of the spectrum makes the spectrum look non-repeatable.

In summary, specimen motion in vibrothermography is proportional to the transducer velocity (with sufficient coupling) and the effect of transducer on overall inspection can be minimized by making the transducer spectrum uniform over a wide bandwidth. This can be achieved by adding an inductor in series with the transducer. The high amplitude behavior of transducer velocity changes significantly with time and usage; resonance peaks shrink in width and the resonances shift towards lower frequencies.

APPENDIX. MATCHED FILTER BASED ALGORITHM APPLIED TO LINEAR CHIRP EXCITATION TO ELIMINATE NOISE AND SEPARATE HARMONICS IN THE SPECTRUM

The transducer behavior becomes nonlinear at high amplitude excitations and various harmonics and sub-harmonics of the excitation frequency appear in the spectrum. For high amplitude tests, we use a matched filter based algorithm to separate the higher order harmonics from the original spectrum. At small signal excitation, the transducer behavior is linear and no harmonics appear, but the signal contains quantization noise arising from the data acquisition process. This algorithm can also be used as a denoising filter to reduce the quantization noise. The algorithm was developed by Ricky Reusser at the ISU CNDE.

In this appendix, we discuss the case when the excitation signal is a linear chirp signal. We use this type of excitation for evaluating the transducer spectrum across a wide frequency range. The transducer is excited with a linear chirp signal of duration 1.0 second with frequency linearly varying from f_{min} to f_{max}. The mathematical definition of linear chirp signal is given in equation .1.

$$r(t) = \cos(2\pi(\overbrace{\frac{1}{2}mt^2 + f_{min}t}^{f(t).t})) \tag{.1}$$

the instantaneous frequency $f(t)$ is given by:

$$f(t) = \frac{d(f(t).t)}{dt} = mt + f_{min}$$

where the slope m is calculated as $\frac{f_{max}-f_{min}}{t_{max}-t_{min}}$. The instantaneous frequency can be calculated using the slope m, and initial frequency f_{min} as:

$$f(t) = f_{min} + mt \tag{.2}$$

To the extent that the system is linear, the transducer output waveforms (velocity and current) should have the same instantaneous frequency as the input excitation signal (voltage). For small signal excitation, this is true, except for the quantization noise originated from data acquisition (or other noise/nonlinearity sources). This high frequency noise can be reduced by using the original excitation waveform (linear chirp) as a reference signal for a matched filter. We use this method for denoising various waveforms for small signal analysis.

At high amplitude excitation, since the transducer behavior is nonlinear, the instantaneous frequency in the output waveforms is not just the original excitation frequency but also its multiples (harmonics) and fractions (sub-harmonics). To extract a particular harmonic component, matched filter is applied with a reference signal whose instantaneous frequency varies as that of the desired component.

A matched filter cross-correlates a known reference signal with an unknown measured signal to detect the presence of the reference signal in the unknown signal. Matched filters are commonly used in radar, in which a known signal is sent out, and the reflected signal is examined for common elements of the outgoing signal. Mathematically, a cross-correlation is equivalent to convolving the unknown signal with a conjugated time-reversed version of the reference signal. The resulting correlation coefficients are the measure of similarity between both signals as a function of lag (time shift). If the two signals are exactly the same, the maximum cross correlation coefficient of 1 occurs at zero lag. If the unknown signal is a shifted version of the reference signal, the maximum value occurs at a lag corresponding to the relative shift. In a linear chirp signal, every frequency within the sweep range has a characteristic time (the duration of the presence of the frequency in the signal). Within this characteristic time, the filter extracts from the measured signal the component of the corresponding frequency. If that particular frequency component exists in the measured signal but not in within its characteristic time, it is still not detected.

This implementation first cross-correlates the reference signal with the measured signal. Due to the wide bandwidth of the frequency sweeps, the components of the measured signal present in the reference signal appear as a band-limited δ-function at zero lag position. A window function is applied to eliminate the unmatched components contained in the sidelobes.

Deconvolution of the windowed function with the original reference signal reconstructs a filtered version of the original signal. To extract the fundamental component, the original excitation waveform is used as a reference signal. Doubling the argument of the cosine function of the reference signal in equation .1 extracts the second harmonic. This is because, for second harmonic generation, the reference signal is the square of the original reference signal. Thus the instantaneous frequency is twice that of original reference signal. This is shown in equation .3. For third harmonic, the argument is thrice that of the original reference signal and so on.

$$r_1(t) = \cos^2 \underbrace{\left(2\pi(\frac{1}{2}mt^2 + f_{min}t)\right)}_{\theta} \tag{.3}$$

$$cos^2\theta = \frac{1}{2} + \frac{1}{2}\cos 2\theta \tag{.4}$$

Apart from harmonic separation, matched filter can also be used as a denoising filter to eliminate the quantization noise from the spectrum. Since the transducer behavior for small signal excitation is linear, it has no higher order harmonics and sub-harmonics. So the high frequency noise can be eliminated by using the original linear chirp excitation waveform as the reference signal for the matched filter and remove any additional frequencies present apart from the input frequencies. We use this method for denoising various waveforms in our small signal analysis.

The mathematical implementation of the algoritm in both time and frequency domain is explained in the table .1

Table .1 Step by step mathematical implementation of matched filter implementation in time and frequency domain

	Time domain	**Frequency domain**
Calculate cross correlation between the reference signal and measured signal	$C(t) = \int_{-\infty}^{\infty} r^*(\tau)x(t+\tau)d\tau$	$R(j\omega) = FFT(r(t))$ $X(j\omega) = FFT(x(t))$ $C(t) = IFFT(X(j\omega)R^*(j\omega))$
Apply a window function to the cross correlation function to eliminate the unmatched signal components	$W(t) = e^{-\frac{1}{2}(\frac{t\omega}{2\pi})^4}$ $C_{windowed}(t) = C(t)W(t)$	
Deconvole the reference signal from the windowed correlation function to get the filtered output		$s(t) = IFFT\left(\frac{FFT(C_{windowed}(t))}{R^*(j\omega)}\right)$

BIBLIOGRAPHY

[1] Henneke E.G., Reifsnider K.L. and Stinchcomb W.W., "Vibrothermography: Investigation, Development, and Application of a New Nondestructive Evaluation Technique" ,*U.S. Army Research Office Final Report*, DAAG29-82-K-0180, pp. 22, 1986.

[2] Uhl C.J., Holland S.D., and Renshaw J., "Vibrothermographic crack heating: a function of vibration and crack size", *Review of Progress in Quantitative Nondestructive Evaluation*, D.O. Thompson and D.E. Chimenti, Eds., Vol 28A, pp. 489, 2009.

[3] Zhang W., Holland S.D., and Renshaw J., "Frequency dependence of Vibrothermography", *Review of Progress in Quantitative Nondestructive Evaluation*, D.O. Thompson and D.E. Chimenti, Eds., Vol 29, pp. 505-509, 2010.

[4] Han X., "Frequency dependence of the thermosonic effect", *Review of Scientific Instruments*, 74:414, 2003.

[5] Zhang W., Holland S.D., "Dependence of Vibrothermographic heating on shear versus normal loading", under review *NDT&E International*.

[6] Renshaw J., Holland S.D., Thompson R.B. and Uhl C.J., "The effect of crack closure on heat generation in Vibrothermography", *Review of Progress in Quantitative Nondestructive Evaluation*, D.O. Thompson and D.E. Chimenti, Eds., Vol 28A, pp. 473, 2009.

[7] Renshaw J., Holland S.D., Anderegg J., Thompson R.B. and Paul R., "Vibration-induced tribological damage to fracture surfaces via vibrothermography", *International Journal of Fatigue*, Vol 33, Issue 7, pp. 849-857.

[8] Favro L.D., Han X., Li L., Zhong O., Sun G., Thomas R.L., and Richards A., "Thermosonic Imaging for NDE", *Review of Progress in Quantitative Nondestructive Evaluation*, D.O. Thompson and D.E. Chimenti, Eds., Vol 20, pp. 478-482

[9] Han X., Li W., Zeng Z., Favro L.D., and Thomas R.L., "Acoustic chaos and sonic infrared imaging", *Applied Physics Letters*, 81:3188, 2002.

[10] Holland S.D., "First measurements from a new broadband vibrothermography measurement system," *Review of Progress in Quantitative Nondestructive Evaluation*, D.O. Thompson and D.E. Chimenti, Eds., Vol 26A, pp. 478-483, 2007.

[11] Elmore W.C. and Heald M.A., *Physics of Waves*, (Dover Publications, Inc., New York, NY, 1985), pp. 114-122.

[12] Ikeda T., *Fundamentals of Piezoelectricity*, (Oxford University Press, Tokyo, 1990), pp.1-3,18-21

[13] Beranek L. L., *"Acoustics"*, (Acoustical Society of America, New York, NY, 1996), pp. 47-62.

[14] Godse A.P, Bakshi U.A, *"Electronic Devices & Circuits - II"*, (Technical Publications, Pune, India, 2008), pp. 352-353.

[15] Boast W.B, *"Principles of Electric and Magnetic Fields"*, (Harper & Brothers, New York, NY, 1956), pp. 250-251.

[16] Zhou D., Kamlah M., and Munz D., "Rate dependence of soft PZT ceramics under electric field loading", *Proc. SPIE* 4333, 64 (2001); doi:10.1117/12.432740